数理物質科学研究科 博士論文の要約

Graduate School of Pure and Applied Sciences

Study on electromagnetic double Dirac cones and topological edge modes in photonic crystal slabs
(フォトニック結晶スラブ中の電磁的二重ディラックコーンとトポロジカルエッジモードの研究)

AFSHAN BEGUM

Doctoral Program in Materials Science and Engineering

Student ID Number: 201930120

Doctor of Philosophy in Engineering

Advised by: Yoshihiko TAKEDA

Abstract

This thesis aims for the experimental verification of double Dirac cones and topological edge modes in photonic crystal slabs by high-precision fabrication. Photonic crystals (PhC) of the C_{6v}-symmetry can materialize double Dirac cones at the center of the first Brillouin zone (FBZ) by the accidental degeneracy of E_1 and E_2 modes created by tuning the structural parameters. Effective refractive index vanishes at the crossing point of Dirac cones called the Dirac point, as two linear dispersions of opposite slopes intersect. They can be utilized for beam shaping and to simulate optical cloaking. Owing to the requirement of fine-tuning structural parameters to achieve accidental degeneracy, physical manifestation of the double Dirac cones is exceedingly difficult. In addition, to measure these dispersions a very small region around the Γ point needs to be probed. In a special case of triangular lattice called the honeycomb lattice, topological bandgaps can be created between the double Dirac cones by distorting a unit cell such that the C_{6v}-symmetry is preserved. Topological edge modes with one-way propagation can be materialized in these bandgaps. These modes have been proposed as waveguides mitigating disorder induced backscattering, but the extent of robustness is yet to be completely understood.

Theoretical studies with finely tuned parameters have been discussed rigorously. However, whether these properties can be materialized in real life with requirements of such high-precision fabrication remains an important question for the possibility of practical applications. The thesis focuses on their investigation by dispersion relation obtained on precisely fabricated specimen. Double Dirac cones were experimentally materialized at the center of the first Brillouin zone (FBZ) by accidental degeneracy, made possible with uniform fabrication of large array PhCs. The linear dispersion of the strongly angle dependent Dirac cones were investigated using high-angle resolution reflection spectroscopy. Polarization selection rules were employed to distinguish modes at Γ point, and we showed two pairs of linear dispersions obtained with opposite sign and nearly equal magnitude. This technique was then applied to observe topological inversion of the E_1 and E_2 modes on PhC slabs at the Γ point, in a purely experimental manner. Complete photonic bandgaps in topologically trivial and non-trivial PhCs were obtained in fabricated specimen with sharp vertices. A process to bury PhCs in cladding material silicon dioxide is developed for hole type PhCs, to create symmetric SOI equivalent of membrane structures but surrounded by low-index material. A model to evaluate formation of air pockets in triangle shaped trenches is presented, which was used to evaluate void volume percent in the buried PhCs. Topological edge states were detected by linearly polarized high angle resolution reflection spectroscopy on specimen made by stitching multiple boundaries of trivial and non-trivial PhCs.

Properties of photonic crystals have been long rigorously theorized, but in this thesis, I demonstrate that the properties could be realized through precise structure fabrication and high-resolution measurement evaluation. The chapters in thesis are summarized below.

Introduction

This chapter describes the background, review of literature and research objectives.

PhC slabs are promising optical systems for manipulating the flow of light, owing to their periodic lattice. C_{6v} symmetric PhCs materialize double Dirac cones at the center of its first Brillouin zone by a spatial combination of E_1 and E_2 modes, which can be applied to steerable antennas, cloaking and sharp bend waveguides. Honeycomb lattice, a special case of triangular lattice can materialize topologically trivial and non-trivial bandgaps, with slight deformation such that C_{6v} symmetry is retained. Topologically protected back reflectionless edge modes can be supported at the physical boundary between such PhCs, making it useful for PhC slab waveguides.

The photonic band summarizes dispersion relation of photonic structures yielding information on modes, spatial mode symmetries and slopes to determine group velocities. Photonic bands have been thoroughly determined theoretically, but with the advanced nanofabrication techniques, it is now possible to fabricate accurate specimen and obtain photonic bands experimentally to test for bandgaps, propagation modes, quality factors, and peak widths, to mention a few. Conventionally, the photonic band is obtained by variable angle transmission or reflection spectroscopy on samples, which is then mapped against wavevector. Depending on the nature of dispersion relation and characteristics to be determined, conditions of spectroscopic methods vary. If the dispersion is linear around the crossing point it exhibits a strong angular dependence whose measurement requires higher angle-resolution than conventional methods. Mode of different spatial symmetries behave differently throughout the FBZ depending on polarization of the incident light and peak width, requiring polarized spectroscopy, engineering of quality factors and/or enhancing signal collection time.

Dirac cones are materialized by accidental degeneracy at the center of the first Brillouin zone by finetuning of structural parameters. Its physical manifestation thus relies on the precise fabrication for careful control of structural parameters, making experimental observation challenging.

Complete photonic bandgaps are created by varying the shape and size of nanostructure in a PhC unit cell which manipulates the effective refractive. A careful curation of parameters during fabrication is required to achieve the designed hole shape, which might otherwise close the photonic bandgap. Membrane structures (with air on either side of the PhC layer) have been of chief interest for photonic waveguides, which are achieved by etching out substrate from beneath the PhCs. It was adopted to utilize high refractive index contrast in the vertical direction to confine light within the PhC layer. Additionally, this system is symmetric about the PhC layer, so the modes are distinctly classified as symmetric and antisymmetric modes, [1]. Topological edge modes, which are created in the common photonic bandgaps of trivial and topological PhCs and localized at the physical boundary between them, have been proposed to mitigate disorder-induced backscattering and provide additional directional control over light. Their dispersion close to the normal incidence appears linear and degenerate, but calculations reveal a very small gap and are not actually degenerate. Experimental investigation for the properties of edge modes and small gap around normal incidence requires high angle-resolutions.

Theoretical investigation on the dispersion relations of ideally designed PhCs has been conducted extensively. However, whether these properties can be materialized in such high-precision requirements in real life fabrication remains a very important challenge for future practical applications. The goal of this thesis is to achieve C_{6v}-symmetric PhC properties of double Dirac cones and topological bandgaps by high precision nanofabrication to make uniform samples

by effective parameter control. Then to probe the photonic band exhibiting high angular dependence around the FBZ center using high angle-resolution reflection spectroscopy. This study then presents a consistent approach to identify spatial mode symmetries at Γ point and interpret the dispersion relation by verifying the observed double Dirac cones. By employing polarization selection rules to the obtained spectra, the dispersions around the Γ point are obtained accurately. The rigorous determination of photonic dispersion is therefore systematically applied to observe topological band inversion at the Γ point, and confirm complete photonic bandgap. Next, I experimentally observe the dispersion relation of topological edge-modes at the boundary between trivial and non-trivial PhCs at high angle-resolution to investigate features around normal incidence.

Double Dirac cones at mid-IR frequencies

This chapter introduces the materializes double Dirac cone by accidental degeneracy of the E_1 and E_2 on the Γ point, in PhCs fabricated on SOI, [2].

The C_{6v} symmetric PhCs, [1], have unique property of materializing a double Dirac cone, [3], [4]. The Dirac cones are natural for periodic structures at the high-symmetry K point in reciprocal periodic lattice, they exist below the light cone and cannot be measured. By structural parameter tuning, the Dirac cones are materialized at the center of the periodic lattice This tuning is called accidental degeneracy, and while many designs have been proposed to materialize them, [5], no one has successfully measured it, owing to the delicate nanofabrication and difficulty in accurate measurements, at the zone-center. One of the recent attempts to observe the double Dirac cones were presented in [6], in triangular lattice PhCs fabricated in SOI wafer. The unit cell consisted of one airhole. The characteristic linear dispersion with slopes of equal magnitude and opposite sign were not observed, despite using the high angle-resolution measurements. It occurred for several reasons, firstly, the neighbouring modes were crowded close to the E_1 and the E_2 modes, influencing the dispersion. Secondly the achieved etch depth of airhole was 288 nm, against a designed value of 240 nm. It created a 40 cm^{-1} discrepancy in the observed E_1 frequency, which is quite small. Third, in the plane of PhC, only one parameter, that is the radius of one airhole could be controlled. To overcome, a seven-hole unit cell with 1.5 μm lattice constant was proposed in the theoretical work [3], having a distorted honeycomb lattice with six identical air holes in silicon, with an additional airhole at the center, along with polarization selection rules for modes at the Γ point in the PhCs of C_{6v} symmetry.

To overcome challenges in fabrication, I made samples with two feature size, [2] using a unit cell comprised of seven air-holes of same depth, [3]. The accidental degeneracy was controlled by two radii instead of one. The PhC unit cell was a distorted honeycomb lattice consisting of six identical air holes in SOI, with $a \neq R/3$, shown in Figure 1 (a), where a is the lattice constant and R is the distance between the centre of the air holes and the centre of the unit cell, having FBZ of Figure 1 (b). The deformation in R shifts the six air holes, and keeps the C_{6v} symmetry. When R is reduced, the E_1 mode has a smaller frequency. A seventh air hole with radius r_2 introduced at the centre of the unit cell, where the electric field of the E_1 mode is densely distributed, increases the E_1-mode frequency eventually crossing the E_2-mode.

I made 3 mm by 3 mm PhC arrays, by conventional CMOS (Complementary metal–oxide–semiconductor)-compatible nanofabrication technique by electron beam lithography (EBL), followed by through etching of the nanostructure using Inductively Coupled Plasma in Reactive Ion Etching (ICP-RIE). By optimizing exposure parameters in EBL, I simultaneously made air holes of radii 90 nm and 336 nm. Then, I performed through etching of 400 nm depth using deep Bosch process achieving same hole depth for both radii, which removed the inaccuracies due to etching depths. I made five samples of unit cell consisting of six constant radius airhole, and varied radius of central air hole from 0 to 168 nm, giving room for fabrication tolerance.

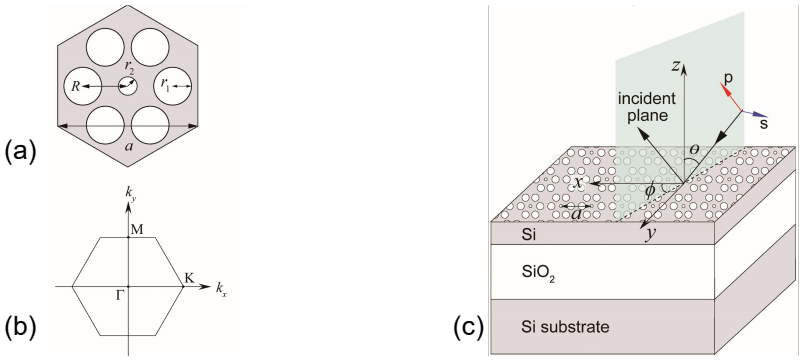

Figure 1. (a) The top view of the unit cell, **(b)** First Brillouin zone of the PhC with C_{6v} symmetry, **(c)** Configuration of the incident plane wave for the angle-resolved reflection measurement, on the illustration of the specimen structure. θ and ϕ denote the tilt angle from the normal (z) direction and the azimuthal angle from the x axis, respectively. s and p denote the polarization directions of the incident electric field, which are perpendicular and parallel to the incident plane, respectively. Two dimensional PhC slabs were fabricated in the top silicon layer of SOI wafers.

During the fabrication, I approached a fine tuning of structural parameters for simultaneous in-plane feature size of approximately 100 nm and 600 nm; maintaining the lattice constant 2.4 μm over a large area of 9 mm^2, and reduced stitching errors. The top-view and cross-section of sample is shown in Figure 2 (a & b), with vertical etched walls of 400 nm height. The etch rate of silicon was 15.6 nm/cycle, smaller than the in-plane air-hole size, creating sufficiently small scallops thus mounting to a low surface roughness without affecting PhC modes.

I used the high-angle resolution measurement set-up, [5], to observe the linear variation of double Dirac cone frequencies with respect to incident angle around the Γ point, and used polarization selection rules, [3], [4], to identify modes of different spatial symmetries. I obtain the slopes from reflection spectra finding two pairs of slopes with nearly equal magnitude of opposite signs in both Γ-to-K and Γ-to-M directions, which are the isotropic linear dispersions of the double Dirac cones. Additionally, I compare the observed reflection peaks with angle-resolved reflection peaks calculated by finite element method (FEM) obtaining a good correlation with experiments.

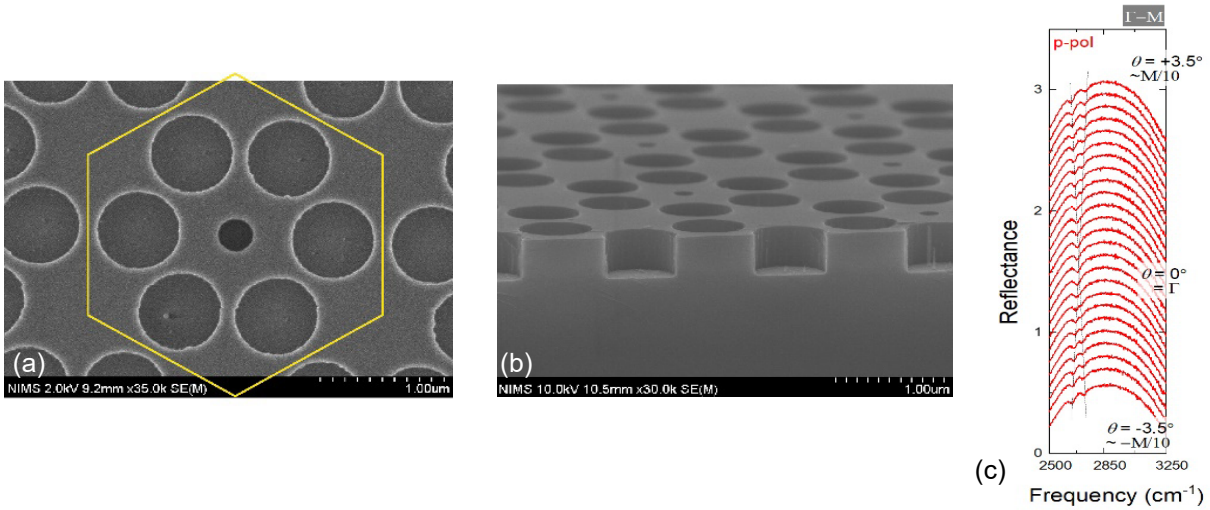

Figure 2. (a) SEM of top-view of a unit cell, and **(b)** the cross-sectional SEM of the PhC slabs fabricated in the top silicon layer of an SOI wafer. **(c)** The reflection spectra of the sample taken in the Γ-to-M direction, measured at a high-angle resolution of 0.3°, from incident angles (= θ) -3.5° to 3.5°.

Before proceeding to the dispersion relations, I used the following poalrization selection rules, [3] to interpret the specimen reflection spectra. The C_{6v} symmetric PhC structure has six mode symmetries, or irreducible representations, on the Γ point, referring to the symmetry of the magnetic field in Table I.

Table I. Selection rules for reflection peaks. p and s denote that the modes are active to p and s polarizations, respectively. E_1 and E_2 modes are doubly degenerate, so there are two branches for each of them in both Γ-to-K and Γ-to-M directions. One branch is active to s polarization and the other is active to p polarization.

Mode on Γ point	Γ ($\theta = 0°$)	Γ-to-K ($\phi = 0°$)	Γ-to-M ($\phi = 90°$)
A_1	inactive	s	s
A_2	inactive	p	p
B_1	inactive	s	p
B_2	inactive	p	s
E_1	active	s, p	s, p
E_2	inactive	s, p	s, p

E_1 and E_2 modes are doubly degenerate, each having two eigenfunctions; and only E_1 mode is active to normal incidence ($\theta = 0°$). These are the key to distinguish E_1 from E_2 modes from neighbouring modes in reflection spectroscopy on PhC. Figure 1 (c) shows the measurement configuration on the PhC slabs.

The dispersion relation is investigated, first at near normal incidence using IR microscope (JASCO, IRT-5200) with FT-IR spectrometer (JASCO, FT/IR-6800). It measures normal incidence reflectance with an angle distribution of ~5°. Second, the dispersion around Γ is examined by the high angle-resolution set-up ($\Delta\theta = 0.3°$) using optical breadboard made by collaborators in [5]. It is integrated in the sample chamber of an FT-IR spectrometer (JASCO 6800). The set-up was previously used to measure the Dirac cone in the square, [7], and triangular-lattice PhCs, [6], and the evaluation of surface-emitting quantum cascade lasers with PhC resonators, [8]. To achieve the high angle-resolution, the beam spot scanning the sample is 2 mm in diameter, and thus the sample is kept larger at 3 mm by 3 mm.

The optical reflectance was obtained by performing linearly polarized reflection spectroscopy in both Γ-to-M and Γ-to-K directions. Figure 2 (c), shows the measured reflection spectra in Γ-to-M direction for incident angles -3.5° to 3.5° at p polarization. The PhC modes appear as sharp peaks of Fano-line shape superimposed on large background undulations. Large undulations are caused by the interference of the Si and SiO_2 layers in the SOI wafer. Two small peaks between frequencies 2500 and 2850 cm^{-1} at incident angle -3.5°, merge at normal incidence ($\theta = 0°$) and reappear at 3.5°, traced by black dotted lines drawn behind the peaks. A similar measurement was obtained for both the polarizations and in the Γ -to-K direction as well.

The slope of the dispersion was obtained in the measurements as $v_g/c = 0.254$ (Γ–K, s), 0.259 (Γ –K, p), 0.262 (Γ –M, s), and 0.257 (Γ –M, p), while the isotropic v_g/c derived from the calculated dispersion relation was 0.2555 ± 0.0032. This revealed the isotropic nature of observed double Dirac cones within margin of errors and the observed reflectance corresponded well with calculated reflectance in accordance with the polarization selection rules.

Topological bandgaps in non-membrane PhC slabs

In this chapter, I investigate topological band inversion in PhCs in mechanically robust silicon-on-insulator instead of conventional fragile membrane structure and characterize the photonic bandgaps by measuring its reflection spectra and mapping the optical dispersion. The topological band inversion is observed at the Γ point and interpreted using polarization selection rules. Traces of edge state are found at the boundary between trivial and non-trivial PhC slabs, [9].

Wu and Hu proposed the scheme to materialize topologically trivial and non-trivial bandgaps, [10], in a honeycomb lattice with six pillars, which is a special case of a triangular lattice. The six pillars equidistant from the centre of a unit

cell naturally have double Dirac cone on the Γ point. When the unit cell is distorted while preserving C_{6v}-symmetry, creates photonic bandgaps of topologically trivial and non-trivial nature. They showed that the boundaries between these two PhCs can support edge modes promising back reflection less systems. Subsequently, such structures were fabricated in thin free standing GaAs membrane and one-way propagation was confirmed by observing photon pair emission from InAs quantum dots under applied magnetic field at two opposite ends of the waveguide, [11]. Sharp-vertices in triangle airholes were used to obtain complete bandgap in the M direction, [12], achieved by a special computer-aided design (CAD) stencil of concave triangles. A regular triangle created rounded vertices during the fabrication which reduced the complete bandgap, [11], [13]. Topological edge modes open new possibilities for optical circuits; however, the extent of topological protection extends to non-membrane systems is yet to be completely understood. Additionally, literature on the investigation of dispersion of edge states exist with circularly polarized incident light. The small gap between edge states at normal incidence is theorized to be linearly polarized and has not been observed du to limited angle resolutions of existing methods.

I apply the systematic technique established in previous chapter to investigate topological bandgaps between the E_1 and E_2 modes of C_{6v}-symmetric PhC slabs on SOI wafer, [9]. I employ polarization selection rules to identify the topological band inversion at the Γ point in a purely experimental manner. I measure complete photonic bandgaps in the Γ-to-M directions, indicating sufficiently sharp vertices achieved in sample fabrication using a regular triangle CAD stencil. I present an evaluation of the extent of sharpness in the fabricated sample, to correlate with the achieved bandgap. I detect traces of edge states in normal incidence the reflection spectroscopy on sample with multiple boundaries with trivial and non-trivial PhCs.

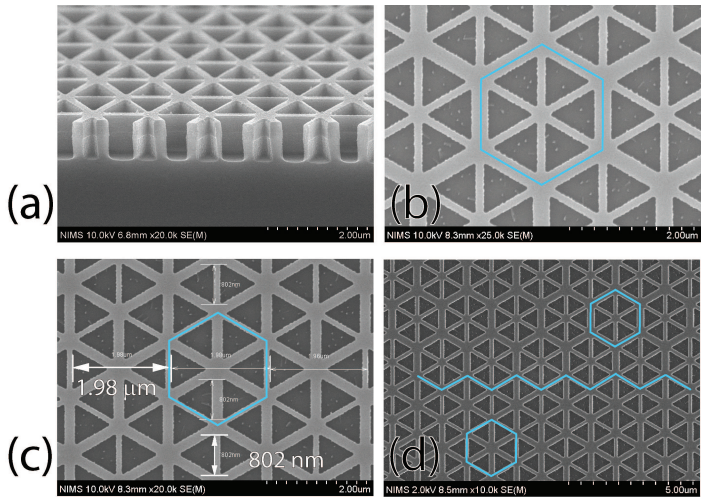

Figure 3. SEM images of fabricated specimens. **(a)** Cross-sectional view after etching. Top view of **(b)** PhC-t and **(c)** PhC-n. **(d)** Top view of the edge-mode specimen. The zig-zag boundary between PhC-t and PhC-n and their unit cells are highlighted by blue lines.

Figure 3 (a) shows the cross-section of fabricated PhCs using a regular CAD stencil. The unit cell consisted of six identical triangular air cylinders in the top silicon layer of the SOI wafers with $a/R = 3$, where a is the lattice constant of the PhC and R is the distance between the centre of the air cylinders and the centre of the unit cell. At this point, I destroy the unit cell from the honeycomb symmetry ($a/R \neq 3$) by pushing the air cylinders towards the centre, but keeping the C_{6v} symmetry, Figure 3 (b). It lifted the degeneracy between E_1- and E_2 modes on the Γ point, with higher frequency of E_2-mode for the trivial PhC (PhC-t). I obtain non-trivial bandgaps by adjusting R, that is by pushing out the air cylinders by

80 nm, Figure 3 (c). It pushed the frequency of E_1-mode higher than E_2-mode (PhC-n). Thus, a photonic bandgap common to both trivial and non-trivial PhCs was obtained.

I probed the photonic bandgaps of these samples by high-resolution angle-resolved reflection spectroscopy in the mid infrared region, whose structures were designed to materialize complete common bandgaps of topologically trivial and non-trivial PhCs for TE (transverse electric)-like modes without under-etching of the top silicon layer. Figure 4 (a) shows the angle resolved reflection spectrum on designed trivial PhC in Γ-to-M direction ($\phi = 90°$). There are two peaks of which the larger intensity is around 3000 cm^{-1} and smaller intensity is around 3250 cm^{-1}. The smaller intensity peak disappears at normal incidence, whereas, larger intensity peak appears even at normal incidence. Following the polarization selection rule at Γ point in Table I, only E_1 mode is active at normal incidence, hence the origin of large intensity peak is E_1 is confirmed. The small intensity peak is active to both s and p polarizations around same frequency, and by following the polarization selection rule, it originates from E_2 mode. On the other hand, Figure 4 (b) is the angle resolved reflection spectra on another specimen in Γ-to-M direction. Here the position of large intensity peak is interchanged, confirming topological inversion. For a wider-angle measurement in complete FBZ, I used the commercial attachment Seagull (Harrick Scientific) for 5 to 70° incident angles.

By applying polarization selection rules expected from the spatial symmetry of the electromagnetic eigenmodes, I confirmed the band inversion on the Γ point. I confirm the complete bandgap in M direction by wide angle reflection measurements using commercial variable angle tool for both PhC-t and PhC-n. This result is conducive to the sharp vertices of triangle airholes achieved in fabrication.

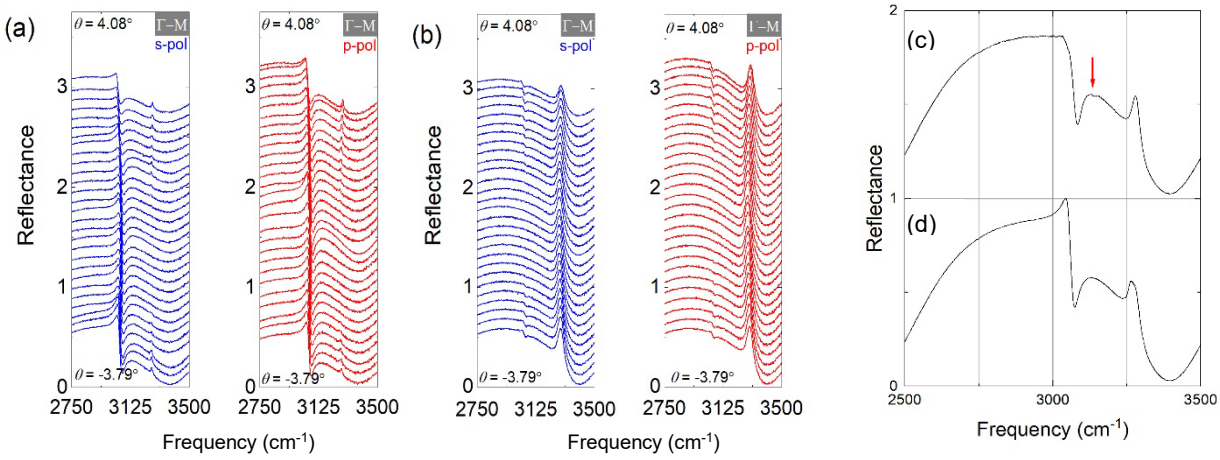

Figure 4. Angle-resolved reflection spectra of **(a)** PhC-t and **(b)** PhC-n measured in the Γ -to-M directions ($\phi = 90°$) for both s and p polarizations by home-made high-resolution setup. Each panel consists of 28 spectra measured for different incident angles (θ) in 0.292° steps. The upper and lower limits of the lowest reflection spectrum in each panel are 1 and 0, respectively. Other spectra are drawn in the same scale and shifted by 0.1 in the vertical direction. **(c)** Normal-incidence reflection spectrum of the edge-mode specimen measured by microscope FT-IR, where the red arrow points a small dip in the common gap frequency range, which may indicate an edge mode on the Γ point. **(d)** The arithmetic average of normal incidence reflection spectra of PhC-t and PhC-n. Two peaks around 3050 and 3300 cm^{-1} show the lower and upper edges of the common gap.

To confirm the topological edge states at the boundary between these PhCs, I fabricated a 4 mm by 4 mm PhC array with combination of PhC-t and PhC-n (Figure 3 (d)) consisting 25-unit cells each on either side of the boundary, and compared with the dispersion relation of edge modes calculated by FEM. I then detected the trace of edge-states at normal incidence using microscope FT-IR reflection measurement. Figure 4 (c) shows the measured trace marked by red arrow,

between two large peaks. The latter are E_1 modes of individual PhC-t and PhC-n (Figure 4 (d)). The frequency of the small undulation is close to the calculated edge mode frequencies at zero wavevector.

I observed the complete bandgap towards the M direction by measuring the reflection spectra. I obtained a bandgap on 5.97 % from the experiments, agreeing with the theoretical bandgap of 5.73 %. This shows that complete bandgap could be achieved in the fabricated sample with the regular CAD stencil, due to smaller rounding off at the edges in my sample. This complete common bandgap is a prerequisite for the existence of topologically protected edge modes. Although the materialization of the edge modes localized on the boundary between the two PhCs was proved by the FEM calculations, only their trace was detected by a focused microscope FT-IR measurement.

Topological bandgaps and edge states in buried PhCs

In this chapter, I investigate topological inversion and edge states by burying PhCs in silicon dioxide, [14]. PhCs are capped with a layer of silicon dioxide by plasma-enhanced chemical vapor deposition (PECVD), same as insulator layer in SOI wafer, making it symmetric about the PhC layer in silicon.

The TE (transverse electric) and TM (transverse magnetic) modes are rigorously separated in the symmetric structures, [1], so membrane structures are conventionally used for rigorous bandgap and utilizing high refractive index contrast of air vs dielectric material. For robust structure with genuine photonic bandgaps, symmetric SOI (silicon-on-insulator) slabs can be used (proposed by Yao [14]), by capping the PhCs with same material as substrate, in this case silicon dioxide. I grow SiO_2 by plasma-enhanced chemical vapor deposition (PECVD), making it symmetric about the silicon layer with PhCs, as shown in the illustration Figure 5 (a). Buried PhCs with pentagonal pillar are being used for vertical emitting PhC lasers, [8], while triangular hole PhCs are employed for topological edge modes, buried in a secondary material. Deposition/growth of silicon dioxide in PhCs of triangle shaped holes is challenging because non-uniform burying results in air pocket (void) formation which can make the photonic bandgap ambiguous.

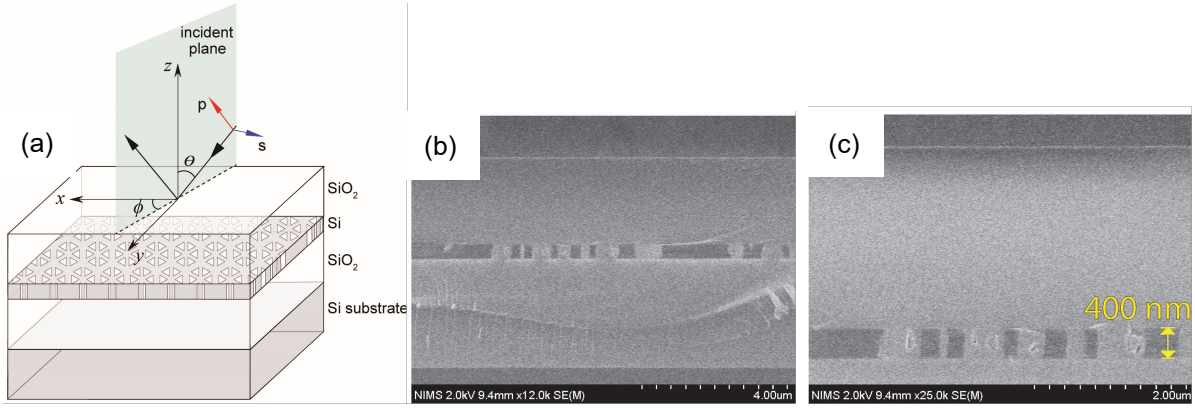

Figure 5. (a) Configuration of the incident plane wave for the angle-resolved reflection measurement on the illustration of the specimen structure. θ and ϕ denote the tilt angle from the normal (z) direction and the azimuthal angle from the x axis, respectively. Two-dimensional PhCs were fabricated in the top silicon layer of SOI wafers and then silicon dioxide was grown over the PhCs **(b)** Cross-sectional SEM of the symmetric SOI specimen after growing silicon dioxide on the PhCs, view of PhC walls buried in the silicon dioxide. **(c)** Close-up of the PhCs, showing minimal void.

To detect topological edge states in symmetric-SOI, I fabricated triangular-shaped airhole PhC slabs buried in silicon dioxide, [14]. I studied the void formation by comparing physical deposition method of sputtering and chemical method of growing silicon dioxide in trenches. I modelled the void fraction by taking effective refractive index (RI) in triangular

hole as combination of air and SiO_2, representing volume fraction of air. An effective RI of 1 was 100 % air, while effective RI of 1.44 was 100 % SiO_2. Then I calculated the E_1 and E_2 frequencies at Γ point, showing the effect of ambiguous bandgap if air pockets exist. Then, by normal incidence spectroscopy on PhCs where only E_1 mode is active, I compared experimental E_1 mode frequency against the calculated to estimate void volume fraction. A method to confirm minimum void was developed, by using FT-IR reflection spectroscopy on the PhCs at normal incidence. Using this technique, SiO_2 deposition was explored by physical methods of sputtering and chemical deposition of CVD. The best deposition with minimal voids were found in SiO_2 grown using PECVD (Figure 5 (b,c)), confirmed by cross sectional SEM of one of the PhCs.

Topologically trivial and non-trivial PhCs with least air pockets were fabricated, on which I experimentally confirmed band inversion at Γ and complete photonic bandgap in the M direction. I covered the combination specimen (with multiple boundaries between PhC-t and PhC-n) and detected edge modes by performing linearly polarized angle-resolved reflection spectroscopy. I obtained their photonic dispersion by curve fitting to confirm linear polarization of edge modes at zero wavevector.

Conclusions & Outlook

In this thesis, I investigated PhC slabs of the C_{6v} symmetry for the experimental verification of double Dirac cones and topological edge modes in photonic crystal slabs by high-precision fabrication. I discussed process to fabricate uniform PhCs with simultaneous fabrication of two feature sizes, and triangle holes with sharp vertices. By applying polarization selection rules I identified mode symmetries, observed topological inversion, and complete photonic bandgaps. I detected topological edge states around zero wavevector in linearly polarized reflection spectroscopy. Through the complete theoretical and experimental investigations, the properties of PhCs around the Γ point are validated. The main conclusions are:

- I developed a framework to determine dispersions around the Γ of the reciprocal lattice and identify mode symmetries. I discussed the systematic evaluation to fabricate uniform PhC slabs of different feature sizes using electron beam lithography and etching. I showed it is possible to materialize double Dirac cones at the Γ point by accidental degeneracy with precise nanofabrication.
- I obtained dispersion relation close to Γ by measuring the angle-resolved reflection spectra at 0.3° angle resolution around normal incidence. I identified various mode symmetries of the C_{6v} PhCs by applying polarization selection rules. Then I observed double Dirac cones with experimental slopes comparable to theoretically predicted slopes, revealing isotropic nature.
- I observed topological bandgaps and edge modes in non-membrane SOI structures having triangle holes. I achieved sharp vertices in fabrication which was crucial for complete photonic bandgaps. Then I confirmed the topological inversion utilizing polarization selection rules and comparing the associated peak intensities in reflectance measurements. I observed edge states on samples constituting repetitive combination of trivial and non-trivial PhCs. I first detected their trace by a focused microscope FT-IR reflectance measurement, then obtained complete dispersion in the angle-resolved reflection spectra of symmetric SOI samples.
- I deposited a uniform layer of silicon dioxide on triangle hole PhCs without air-pockets. I developed a method to confirm minimum void formation combining reflection spectroscopy with polarization selection rules. To check the fabrication accuracy of PhCs, I combined measuring reflectance at normal incidence, where only E_1 mode is active to compare the agreement between observed and calculated E_1 frequencies.

- I detected edge modes in linearly polarized angle-resolved reflection spectroscopy around zero wavevector and confirmed a previous theoretical prediction of linear polarization at zero wavevector.

The thesis contributes to the understanding of the PhCs by evaluation of photonic dispersion around the zone centre of the FBZ using polarization selection rules. It shows materialization of double Dirac cones by effective parameter tuning. The non-membrane structures are evaluated for topological bandgaps and edge states. Properties of photonic crystals have been long rigorously theorized and in this thesis, I demonstrated that the properties could be realized through precise structure fabrication and high angle-resolution evaluation.

References

[1] K. Sakoda, Optical Properties of Photonic Crystals, Springer, 2004.

[2] A. Begum, Y. Yao, T. Kuroda, E. Watanabe, N. Ikeda, Y. Sugimoto, Y. Takeda and K. Sakoda, "Observation of Two-dimensional Isotropic Double Dirac Cones in the Electromagnetic Dispersion Relation," *Journal of Physical Society of Japan,* vol. 91, p. 084401, 2022.

[3] Y. Yao, T. Kuroda, N. Ikeda, T. Mano, H. Koyama, Y. Sugimoto and K. Sakoda, "Angle-resolved reflection spectra of Dirac cones in triangular-lattice photonic crystal slabs," *Optics Express,* vol. 28, p. 21601, 2020.

[4] K. Sakoda, "Double Dirac cones in triangular-lattice metamaterials," *Opt. Express,* vol. 20, p. 9925, 2012.

[5] T. Kuroda, S. Chalimah, Y. Yao, N. Ikeda, Y. Sugimoto and K. Sakoda, "Apparatus for High-Precision Angle-Resolved Reflection Spectroscopy in the Mid-Infrared Region," *Applied Spectroscopy,* vol. 75, p. 259, 2021.

[6] S. Chalimah, Y. Yao, N. Ikeda, Y. Sugimoto, T. Mano, T. Kuroda and K. Sakoda, "Eigenmode symmetry assignment of triangular-lattice photonic crystal slabs and their Dirac cones materialized by effective degeneracy in the mid-infrared region," *Optics Express,* vol. 29, p. 19486, 2021.

[7] Y. Yao, N. Ikeda, T. Kuroda, T. Mano, H. Koyama, Y. Sugimoto and K. Sakoda, "Mid-IR Dirac-cone dispersion relation materialized in SOI photonic crystal slabs," *Optics Express,* pp. 4194-4203, 2020.

[8] S. Chalimah, Y. Yao, N. Ikeda, Afshan Begum, K. Kaneko, R. Hashimoto, T. Kakuno, S. Saito, T. Kuroda, Y. Sugimoto and K. Sakoda, "Mid-infrared angle-resolved spectral characteristics of photonic crystal slabs for application in surface-emitting quantum cascade lasers," *Journal of Nonlinear Optical Physics and Material,* vol. 31, p. 250017, 2022.

[9] Afshan Begum, Y. Yao, T. Kuroda, Y. Takeda, N. Ikeda, Y. Sugimoto, T. Mano and K. Sakoda, "Design and observation of topological bandgaps and edge modes in SOI photonic crystal slabs," *Journal of Physical Society of Japan,* in review.

[10] L.-H. Wu and X. Hu, "Scheme for Achieving a Topological Photonic Crystal by Using Dielectric Material," *Physical Review Letters,* vol. 114, no. 223901, 2015.

[11] S. Barik, A. Karasahin, C. Flower, T. Cai, H. Miyake, W. DeGottardi, M. Hafezi and E. Waks, "A topological quantum optics interface," *Science 359,* vol. 359, pp. 666-668, 2018.

[12] S. Barik, H. Miyake, W. DeGottardi, E. Waks and M. Hafezi, "Two-dimensionally confined topological edge states in photonic crystals," *New Journal of Physics,* vol. 18, p. 113013, 2016.

[13] S. Okada, T. Amemiya, H. Kagami, Y. Wang, N. Nishiyama and X. Hu, "Discussion on fabrication accuracy of infrared topological photonic structures using hyperspectral Fourier image spectroscopy," *Journal of the Optical Society of America B,* vol. 39, no. 9, pp. 2464-2469, 2022.

[14] Afshan Begum, Y. Yao, T. Kuroda, N. Ikeda, Y. Sugimoto, Y. Takeda, T. Mano and K. Sakoda, "Topological bandgaps and edge modes materialized by symmetric SOI photonic crystal slabs in the mid IR range," *Physical Review A,* in review.